View metadata, citation and similar papers at core.ac.uk

brought to you by CORE

provided by Bilkent University Institutional Repository

Thin Solid Films 518 (2010) 5572–5575

Contents lists available at ScienceDirect

Thin Solid Films

journal homepage: www.elsevier.com/locate/tsf

Double subband occupation of the two-dimensional electron gas in $In_xAl_{1-x}N$/AlN/GaN/AlN heterostructures with a low indium content ($0.064 \leq x \leq 0.140$) barrier

S.B. Lisesivdin [a,b,*], P. Tasli [b], M. Kasap [b], M. Ozturk [a], E. Arslan [a], S. Ozcelik [b], E. Ozbay [a,c,d]

[a] Nanotechnology Research Center, Bilkent University, Bilkent, 06800 Ankara, Turkey
[b] Department of Physics, Faculty of Science and Arts, Gazi University, Teknikokullar, 06500, Ankara, Turkey
[c] Department of Physics, Bilkent University, Bilkent, 06800 Ankara, Turkey
[d] Department of Electrical and Electronics Engineering, Bilkent University, Bilkent, 06800 Ankara, Turkey

ARTICLE INFO

Article history:
Received 24 June 2009
Received in revised form 17 April 2010
Accepted 30 April 2010
Available online 8 May 2010

Keywords:
Indium aluminum nitride
Metal organic chemical vapor deposition
Two dimensional electron gas
Hall effect

ABSTRACT

We present a carrier transport study on low indium content ($0.064 \leq x \leq 0.140$) $In_xAl_{1-x}N$/AlN/GaN/AlN heterostructures. Experimental Hall data were carried out as a function of temperature (33–300 K) and a magnetic field (0–1.4 T). A two-dimensional electron gas (2DEG) with single or double subbands and a two-dimensional hole gas were extracted after implementing quantitative mobility spectrum analysis on the magnetic field dependent Hall data. The mobility of the lowest subband of 2DEG was found to be lower than the mobility of the second subband. This behavior is explained by way of interface related scattering mechanisms, and the results are supported with a one-dimensional self-consistent solution of non-linear Schrödinger–Poisson equations.

© 2010 Elsevier B.V. All rights reserved.

1. Introduction

GaAlN/GaN-based field effect transistors have been extensively studied due to the availability of high power and high frequency applications even at high temperatures [1]. Several improvements have been made in the growth and layer structures of the system, such as AlN buffer growth [2] and AlN interlayer insertion at the interface of 2DEG [3]. In addition to GaAlN/GaN-based heterostructures, InAlN/GaN and InAlN/InGaN-based heterostructures were also proposed as a successor of GaAlN/GaN-based heterostructures because of their higher sheet carrier densities, which are provided by the spontaneous polarization of these systems [4,5]. With the higher carrier densities, the occupation of more than one subband may occur. Because of the highly polar structure of these materials, the electron interactions of each subband with interface related scattering mechanisms would be different [6]. Therefore, investigations of the transport properties of each subband have a great importance in producing better devices that have higher mobilities and higher carrier densities. Recently, Gonschorek et al. [7] reported two subband occupancy in $In_xAl_{1-x}N$/GaN-based structures with low indium ($0.03 \leq x \leq 0.23$) barriers.

Herein, we present a study on $In_xAl_{1-x}N$/AlN/GaN/AlN heterostructures ($0.064 \leq x \leq 0.140$) that were grown with metal organic chemical vapor deposition (MOCVD) with very high sheet carrier densities (up to $\sim 7.46 \times 10^{13}$ cm^{-2} at 33 K). We studied temperature dependent Hall measurements, and we proved two subband occupancy in most of the samples via the quantitative mobility spectrum analysis (QMSA) method and one-dimensional (1D) self-consistent solution of non-linear Schrödinger–Poisson equations.

2. Experimental details

The $In_xAl_{1-x}N$/AlN/GaN heterostructures on *c*-plane (0001) Al_2O_3 substrates were grown in a low-pressure MOCVD reactor. Prior to the epitaxial growth, Al_2O_3 substrates were annealed at 1100 °C for 10 min in order to remove surface contamination. The growths were initiated with a 10-nm-thick low-temperature (840 °C) AlN nucleation layer. Then, 460-nm high-temperature AlN buffer layers were grown at a temperature of 1150 °C. A 500-nm-thick undoped GaN buffer layer was then grown at 1070 °C with a reactor pressure of 200 mbars. After the GaN buffer layers, a ~2-nm-thick AlN interlayer was grown at 1085 °C with a pressure of 50 mbars. Then, $In_xAl_{1-x}N$ layers with low indium content were grown under various temperatures (770–830 °C) for different samples at 50 mbars. Finally, ~3-nm-thick GaN cap layer growths were carried out at a temperature of 1085 °C at the same pressure. All of the layers are nominally undoped.

The thicknesses and indium contents of the barrier layers were determined by high-resolution X-ray diffraction (HRXRD) measurements. HRXRD measurements were taken with D8-Discover diffractometer equipped with a monochromator with four Ge (220) crystals for a $CuK_{\alpha1}$ X-ray beam ($\lambda = 1.5406$ Å). The resolution of the ω–θ measurements (where ω and 2θ are the angles of the sample and detector relative to the incident X-ray beam) was 18″ (~0.005°).

* Corresponding author. Nanotechnology Research Center, Bilkent University, Bilkent, 06800 Ankara, Turkey.
E-mail address: sblisesivdin@gmail.com (S.B. Lisesivdin).

0040-6090/$ – see front matter © 2010 Elsevier B.V. All rights reserved.
doi:10.1016/j.tsf.2010.04.120

The thicknesses of the barrier layers (t) were estimated by using $t=\lambda/2\delta\cos\theta_B$ [8]. Here, δ and θ_B are full width at half maximum (FWHM) and the angular position of the peak of the barrier layer, respectively.

For the calculations of the indium content of InAlN barrier layers, Bragg's law is used,

$$2d\sin\theta_B = n\lambda. \tag{1}$$

Here, d is the spacing of the related reflection planes. For hexagonal crystals, d can be calculated for any ($hkil$) plane with

$$d = \frac{1}{\sqrt{\frac{4}{3}\frac{h^2+hk+l^2}{a^2}+\frac{l^2}{c^2}}}. \tag{2}$$

Here, a and c are the lattice parameters of the hexagonal crystal. For the measured (0002) plane, Eq. (2) can be simplified to $d=c/2$. Therefore, the lattice parameter of the AlInN barrier layer can be calculated with Eqs. (1) and (2). With the help of Vegard's law and the known lattice parameters of AlN and InN crystals, the indium content of the AlInN barrier layer was determined. The growth temperatures, thicknesses, and indium content of the barrier layers are shown in Table 1.

By means of Hall measurements with van der Pauw geometry, the temperature and magnetic field (0–1.4 T) dependent mobilities as well as sheet carrier densities were all taken. Contacts were prepared as four evaporated Ti/Al/Ni/Au contacts at the corners. Using gold wires and indium soldering, the electrical contacts were prepared and the ohmic behaviors were confirmed by the current voltage characteristics before the Hall measurements. Because of the single field Hall effect, the measurements only give averaged mobility and carrier concentration information, and these measurements can only be used in those cases of single electron, hole conduction, or single subband conduction in the semiconductor. The case with more than one type of carrier in the investigated sample is called mixed conduction. The correct transport parameters of the individual carriers in mixed conduction can be determined with the magnetic field dependent resistivity and Hall effect measurements. Different magnetic field dependent methods such as the two-carrier fit, multi carrier fit, and mobility spectrum analysis methods have been introduced by several groups for mixed conductivity analyses [9–12].

In the present study, we used the QMSA method for the analyses of magnetic field dependent resistivity and Hall data [13]. The QMSA method is widely used in many studies to extract the mobilities and carrier densities of different carriers in semiconductor materials, including bulk samples, thin films, quantum wells, and multilayer device structures [14–17]. In addition, the mobilities and carrier densities of individual 2D and 3D electrons and holes in GaN-based heterostructures are reported with the implementation of the QMSA method [18,19].

Table 1
Growth temperatures, thicknesses, and the indium content of the InAlN layers in the investigated samples.

Sample	$In_xAl_{1-x}N$ layer		
	Growth temperature (°C)	Thickness (nm)	Indium content (mol%)
A	800	9.3 ± 0.3	10.6 ± 0.2
B	830	9.3 ± 0.3	9.2 ± 0.2
C	770	11.1 ± 0.4	14.0 ± 0.2
D	810	10.8 ± 0.4	6.4 ± 0.2

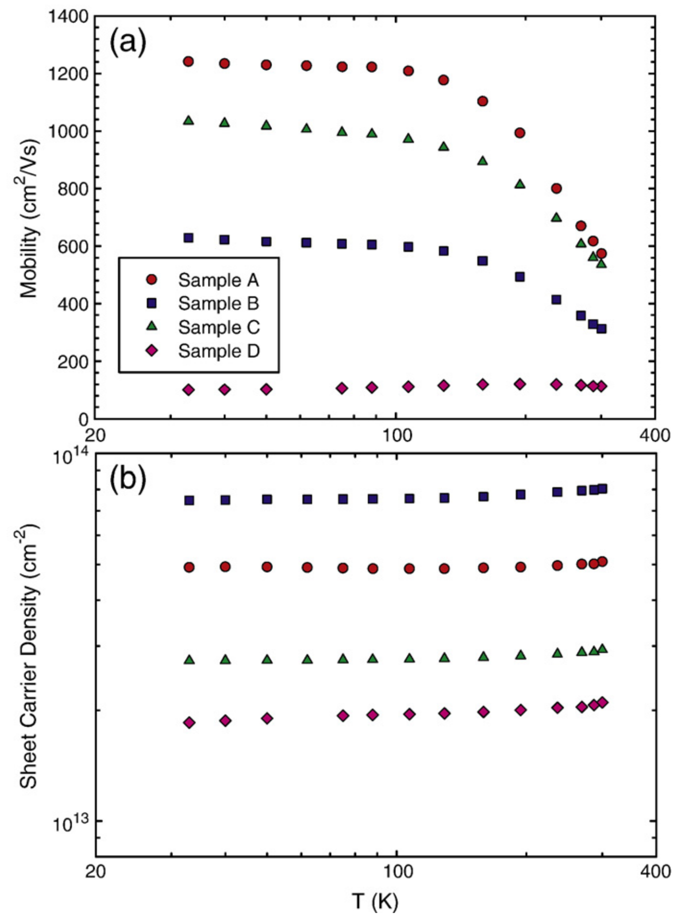

Fig. 1. Temperature dependent (a) Hall mobilities and (b) Hall sheet carrier densities taken at 0.4 T.

3. Results and discussion

Fig. 1 shows the temperature dependence of Hall mobilities (μ_H) and Hall sheet carrier densities (n_H) of the investigated samples at 0.4 T in the temperature range of 33–300 K. The mobilities exhibited temperature independence under 100 K, in which the carrier densities were temperature independent within the studied temperature range. At high temperatures, the mobilities are highly limited by the polar optical phonon scattering mechanism [20]. It is clear that these mobility and carrier density behaviors are typical for those samples where two-dimensional conduction is dominant [21].

In order to extract individual carrier types in the samples, QMSA analysis was performed on magnetic field dependent Hall data at each temperature step for every sample. Fig. 2 shows the QMSA results for sample A. Two distinct electron carriers and a hole carrier were observed in the investigated temperature range.

The maximum magnetic field is better at a range of $B_{max}\approx\mu_{min}^{-1}$ for the extraction of carriers with the mobility spectrum analysis method. Here, μ_{min} is the minimum mobility of a carrier that can be extracted. For the QMSA studies, the $B_{max}\approx 0.5\mu_{min}^{-1}$ condition can be accepted as a limit [22]. For the present study, this condition seems to be barely satisfied, in which the results scatter in the QMSA data.

In a previous study, we presented extracted two-dimensional electron gas (2DEG) and two-dimensional hole gas (2DHG) carriers with low mobilities in an AlGaN/GaN/AlN heterostructure grown on sapphire [23]. In the present study, two distinct electron carriers and a hole carrier show 2D behavior with respect to the previous study. Temperature independent carrier densities for the low mobility 2DEG, high mobility 2DEG, and 2DHG carriers were found as 3.05×10^{13}, 4.95×10^{12}, and 2.53×10^{11} cm^{-2}, respectively. These two 2DEG

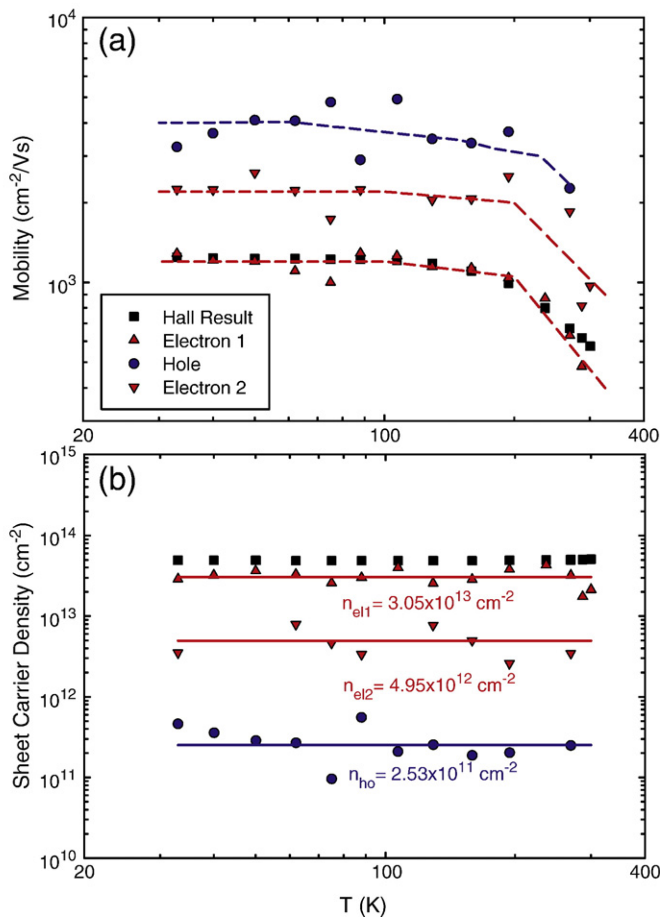

Fig. 2. Mobilities (a) and sheet carrier densities (b) of the extracted carriers obtained from QMSA for the sample prepared at 800 °C. Continuous line represents the average carrier density. The dashed lines shown are guides for the eye.

carriers can be considered as the carriers populated at the first two subbands of a 2DEG system, which are located at the InAlN/AlN/GaN interface. 2DHG is populated at the GaN buffer/AlN buffer [23]. Because of an increase in the 2DHG mobility at low carrier densities via acoustic and interface roughness scatterings [20], and the absence of alloy scattering at the GaN/AlN interface, the mobility of the hole carrier is slightly higher than the mobility of electron carriers.

For GaAs-based multisubband occupied 2DEG systems, the lower subband is expected to have higher carrier density and also higher mobility [24], except for the case of high impurity diffusing into a two-dimensional channel [25]. In this study, the carrier with higher carrier density has lower mobility. For GaN-based systems, this phenomenon is explained by Zheng et al. with the non-uniformity piezoelectric field distribution at the interface [6]. A possible partial strain relaxation at the interface will cause a non-uniform piezoelectric field distribution. This non-uniform polarization field will act as strong scattering centers. Therefore, the first subband has a higher carrier density but lower mobility in GaN-based systems.

In $In_xAl_{1-x}N$/AlN/GaN ($x \sim 0.18$) samples, the effects of the thickness of the AlN interlayer on the electron transport properties were investigated by Teke et al. [26]. For the $x \sim 0.18$, the $In_xAl_{1-x}N$ layer is lattice-matched with the GaN layer and, therefore, the AlN interlayer is the only layer that causes strain at the interface. In this study, the indium content is lower than $x < 0.18$. Therefore, with a higher Al content in InAlN layer, the strain difference between InAlN and AlN is expected to be lower. However, the total strain at the 2DEG interface is expected to be higher due to the additional strain that is induced by the InAlN layer. A simple estimation for the critical thickness for the strain relaxation limit is given by the relation $t_{cr} \approx b_e/2\varepsilon_{xx}$ [7]. Here, b_e is the Burger's vector [27] and ε_{xx} is the in-plain strain. We assume a total homogeneous strain over the GaN layer, which includes the strain values of every layer over the GaN layer. With the help of strain values calculated with the known lattice parameters of AlN and InN, InAlN thicknesses, and nominal AlN interlayer thicknesses, critical thicknesses for every sample are calculated and listed in Table 2. Because the critical thickness of sample grown at 800 °C is nearly the same as the total thicknesses of the InAlN barrier and AlN interlayer, a highly strained interface is expected and highly strained samples are expected to have higher mobilities. In sample grown at 830 °C, the lower indium content causes a higher strain and strain relaxation may occur in this sample. The sample grown at lower temperature (770 °C) has the largest critical thickness, which is far from the actual total thickness. This sample has less strain at the 2DEG interface than the sample grown at 800 °C. Finally, the sample grown at 810 °C has the lowest indium content. Therefore, it has the smallest critical thickness value. This sample's total thickness is drastically above the strain relaxation limit. The interface roughness, due to strain relaxation, is expected to reduce the mobility in this sample [20]. These expectations are highly linked with Fig. 1, which has an order in the sample mobilities as $\mu_A > \mu_B > \mu_C > \mu_D$ at low temperatures.

In Fig. 3, the results of 1D self-consistent solution of non-linear Schrödinger–Poisson equations for Sample A is shown. Simulation steps and more information can be found in a previous study [28]. The material parameters of the $In_xAl_{1-x}N$ layer in the simulation were deduced by using Vegard's law and by using the parameters of InN and AlN. In Fig. 3, the calculated conduction and valence band structures are shown. As observed from the experimental results, a clear 2DEG formation with two populated subbands and a 2DHG formation are calculated. A detailed view of the pseudotriangular quantum well of 2DEG is shown in a box. Because of the pseudotriangular structure of the quantum well, the electron wave function of the first subband is more confined near the interface than the second subband. Therefore, the first subband will be more scattered by non-uniform polarization field scattering as well as interface roughness scattering. Therefore, the mobility of the second subband will be higher than the first subband.

In order to see the change in the carrier densities of these subbands, all of the analysis was extended to all the samples that we measured. The results are shown in Fig. 4. With increasing n_H, a second subband was populated after $n_H > 1.93 \times 10^{13}$ cm^{-2}. The carrier densities of the subbands increase with increasing n_H. The carrier densities of the 2DHG well at ~2 μm deep below the surface are more independent of n_H because of the unchanged conditions for the 2DHG related layers for all the samples.

Table 2
Calculated in-plane strains (ε_{xx}), critical thicknesses and strain relaxation expectations for the investigated samples.

Sample	Growth temperature (°C)	Calculated ε_{xx} at AlN/GaN interface ($\times 10^{-3}$)	Critical thickness (t_{cr}) (nm)	Expectations
A	800	14.7 ± 0.2	10.8 ± 0.2	Highly strained
B	830	15.9 ± 0.2	10.0 ± 0.2	Strain relaxation may occur
C	770	9.0 ± 0.1	17.6 ± 0.1	Strained
D	810	19.7 ± 0.2	8.1 ± 0.2	Above strain relaxation limit

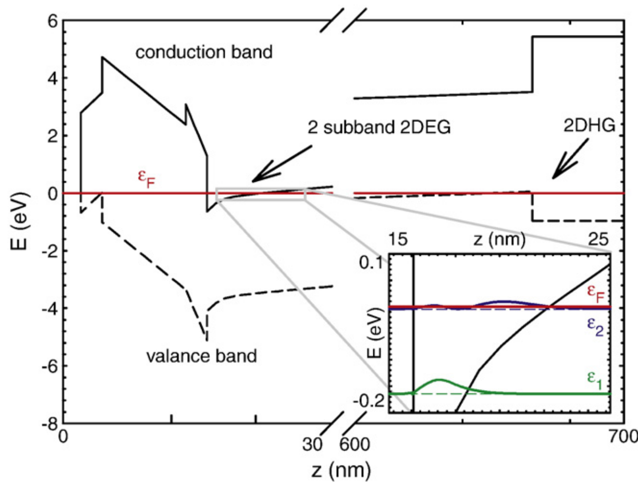

Fig. 3. The 1D self-consistent solution of non-linear Schrödinger–Poisson equations for sample prepared at 800 °C. 2DEG with two subbands and a 2DHG were observed.

4. Conclusion

As a conclusion, the transport properties of the subbands of InAlN-based systems can be analyzed via the implementation of the QMSA method, even by using low magnetic fields at high lattice temperatures. It was found that a second subband begins to populate above $n_H > 1.93 \times 10^{13}$ cm^{-2} for the investigated samples. For the GaN-based heterostructures, it is shown that the electrons in the lowest subband interact with the interface related scattering mechanisms more than the second subband's electrons. Therefore, for those GaN-based devices with a higher mobility-carrier density product, investigating multisubband heterostructures, *i.e.* InAlN/GaN heterostructures with low indium content barriers, shows great importance.

Acknowledgements

This work is supported by the State Planning Organization of Turkey under Grant No. 2001K120590, by the European Union under the projects EU-PHOME and EU-ECONAM, and TUBITAK under the Project Nos. 106E198, 107A004, and 107A012. One of the authors (Ekmel Ozbay) acknowledges partial support from the Turkish Academy of Sciences.

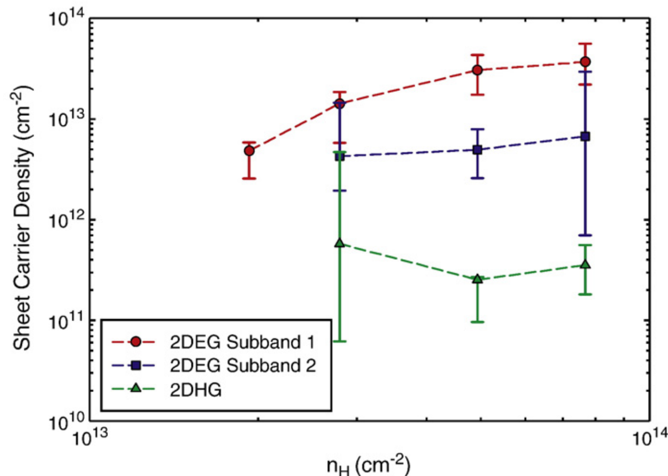

Fig. 4. Sheet carrier densities of 2DHG and the 2DEG subbands with respect to the total sheet carrier density. The dashed lines shown are guides for the eye.

References

[1] Y.-F. Wu, B.P. Keller, P. Fini, S. Keller, T.J. Jenkins, L.T. Kehias, S.P. Denbaars, U.K. Mishra, IEEE Electron. Device Lett. 19 (1998) 50.
[2] S. Yoshida, S. Misawa, S. Gonda, J. Vac. Sci. Technol. B 1 (1983) 250.
[3] L. Shen, S. Heikman, B. Moran, R. Coffie, N.-Q. Zhang, D. Buttari, I.P. Smorchkova, S. Keller, S.P. DenBaars, U.K. Mishra, IEEE Electron. Device Lett. 22 (2001) 457.
[4] J. Kuzmik, IEEE Electron. Device Lett. 22 (2001) 501.
[5] S. Yamaguchi, M. Kosaki, Y. Waranabe, S. Mochizuki, T. Nakamura, Y. Yukawa, S. Nitta, H. Amano, I. Akasaki, Phys. Status Solid A 188 (2001) 895.
[6] Z.W. Zheng, B. Shen, C.P. Jiang, Y.S. Gui, T. Someya, R. Zhang, Y. Shi, Y.D. Zheng, S.L. Guo, J.H. Chu, Y. Arakawa, J. Appl. Phys. 93 (2003) 1651.
[7] M. Gonschorek, J.-F. Carlin, E. Feltin, M.A. Py, N. Grandjean, V. Darakchieva, B. Monemar, M. Lorenz, G. Ramm, J. Appl. Phys. 103 (2008) 093714.
[8] V.V. Mamutin, T.V. Shubina, V.A. Vekshin, V.V. Ratnikov, A.A. Toropov, S.V. Ivanov, M. Karlsteen, U. Sodervall, M. Willander, Appl. Surf. Sci. 166 (2000) 87.
[9] M.J. Kane, N. Apsley, D.A. Anderson, L.L. Taylor, T. Kerr, J. Phys. C: Solid State Phys. 18 (1985) 5629.
[10] M.C. Gold, D.A. Nelson, J. Vac. Sci. Technol. A 4 (1986) 2040.
[11] W.A. Beck, J.R. Anderson, J. Appl. Phys. 62 (1987) 541.
[12] J.S. Kim, D.G. Seiler, W.F. Tseng, J. Appl. Phys. 73 (1993) 8324.
[13] B.C. Dodrill, J.R. Lindemuth, B.J. Kelley, G. Du, J.R. Meyer, Comp. Semicond. 7 (2001) 58.
[14] J.R. Meyer, C.A. Hoffman, J. Antosewski, L. Farone, J. Appl. Phys. 81 (1997) 709.
[15] J. Antoszewski, D.J. Seymur, L. Faraone, J.R. Meyer, C.A. Hoffman, J. Electron. Mater. 24 (1995) 1255.
[16] J. Antoszewski, L. Faraone, I. Vurgaftman, J.R. Meyer, C.A. Hoffman, J. Electron. Mater. 33 (2004) 673.
[17] M. Kasap, S. Acar, Phys. Status Solid A 201 (2004) 3113.
[18] S.B. Lisesivdin, A. Yildiz, S. Acar, M. Kasap, S. Ozcelik, E. Ozbay, Appl. Phys. Lett. 91 (2007) 102113.
[19] N. Biyikli, J. Xie, Y.-T. Moon, F. Yun, C.-G. Stefanita, S. Bandyopadhyay, H. Morkoc, I. Vurgaftman, J.R. Meyer, Appl. Phys. Lett. 88 (2006) 142106.
[20] D. Zanato, S. Gokden, N. Balkan, B.K. Ridley, W.J. Schaff, Semicond. Sci. Technol. 19 (2004) 427.
[21] S.B. Lisesivdin, S. Demirezen, M.D. Caliskan, A. Yildiz, M. Kasap, S. Ozcelik, E. Ozbay, Semicond. Sci. Technol. 23 (2008) 095008.
[22] I. Vurgaftman, J.R. Meyer, C.A. Hoffman, D. Redfern, J. Antoszewski, L. Faraone, J.R. Lindemuth, J. Appl. Phys. 84 (1998) 4966.
[23] S. Acar, S.B. Lisesivdin, M. Kasap, S. Ozcelik, E. Ozbay, Thin Solid Films 516 (2008) 2041.
[24] H. van Houten, J.G. Williamson, M.E.I. Broekaart, C.T. Foxon, J.J. Harris, Phys. Rev. B 37 (1988) 2756.
[25] Y. Gui, S. Guo, G. Zheng, J. Chu, X. Fang, K. Qui, X. Wang, Appl. Phys. Lett. 76 (2000) 1309.
[26] A. Teke, S. Gokden, R. Tulek, J.H. Leach, Q. Fan, J. Xie, U. Ozgur, H. Morkoc, S.B. Lisesivdin, E. Ozbay, New J. Phys. 11 (2009) 063031.
[27] J. Singh, Physics of Semiconductors and Their Heterostructures, McGraw-Hill, New York, 1992, p. 734.
[28] S.B. Lisesivdin, A. Yildiz, M. Kasap, Optoelectron. Adv. Mater. — Rapid Commun. 1 (2007) 467.